LAWRENCE
LIVERMORE
NATIONAL
LABORATORY

UCRL-BOOK-204442

# High Pressure Materials Research: Novel Extended Phases of Molecular Triatomics

C-S. Yoo

June 2, 2004

Chemistry in Extreme Conditions

# High Pressure Materials Research: Novel Extended Phases of Molecular Triatomics

**Choong-Shik Yoo**

Lawrence Livermore National Laboratory, Livermore, California 94551, USA

## 1. HIGH PRESSURE MATERIALS RESEARCH

Application of high pressure significantly alters the interatomic distance and thus the nature of intermolecular interaction, chemical bonding, molecular configuration, crystal structure, and stability of solid [1]. With modern advances in high-pressure technologies [2], it is feasible to achieve a large (often up to a several-fold) compression of lattice, at which condition material can be easily forced into a new physical and chemical configuration [3]. The high-pressure thus offers enhanced opportunities to discover new phases, both stable and metastable ones, and to tune exotic properties in a wide-range of atomistic length scale, substantially greater than (often being several orders of) those achieved by other thermal (varing temperatures) and chemical (varying composition or making alloys) means.

Simple molecular solids like $H_2$, C, $CO_2$, $N_2$, $O_2$, $H_2O$, CO, $NH_3$, and $CH_4$ are bounded by strong covalent intramolecular bonds, yet relatively weak intermolecular bonds of van der Waals and/or hydrogen bonds. The weak intermolecular bonds make these solids highly compressible (i.e., low bulk moduli typically less than 10 GPa), while the strong covalent bonds make them chemically inert at least initially at low pressures. Carbon-carbon single bonds, carbon-oxygen double bonds and nitrogen-nitrogen triple bonds, for example, are among the strongest. These molecular forms are, thus, often considered to remain stable in an extended region of high pressures and high temperatures. High stabilities of these covalent molecules are also the basis of which their mixtures are often presumed to be the major detonation products of energetic materials as well as the major constituents of giant planets. However, their physical/chemical stabilities are not truly understood at those extreme pressure-temperature conditions. In fact, an increasing amount of experimental evidences contradict the assumed stability of these materials at high pressures and temperatures.

Figure 1 illustrates the principle Hugoniots of simple molecules like $O_2$, CO, $N_2$, and $CO_2$ [4]. Clearly, all these materials exhibit the cusps on their Hugoniots at the pressure range between 20 and 40 GPa. At these pressures, these materials could heat up to several thousand degrees because of their high compressibilities. The calculated shock temperature of carbon dioxide, for instance, is about 4500 K at 40 GPa. The presence of such a distinctive cusp on the Hugoniot is surely an indication for chemical reaction or phase change. In fact, many previous statistical mechanical calculations have shown that these materials undergo strong chemical changes such as the decomposition of $CO_2$ and CO to the elementary products like carbon and oxygen and the dissociation of $N_2$ and $O_2$ to diatomic/monatomic ionic products. Note that the Hugoniots of unreacted CO and $N_2$ are nearly identical, attributing to their isoelectronic characteristics resulting in same initial density and similar nonbonded atom-atom potential. The previous diamond-anvil cell studies of these materials [5-7] also found very similar phase diagrams with many isostructural polymorphs. In the later chapter, we shall also see a similar parallelism existing in the phase diagrams of isoelectronic triatomics $CO_2$ and $N_2O$.

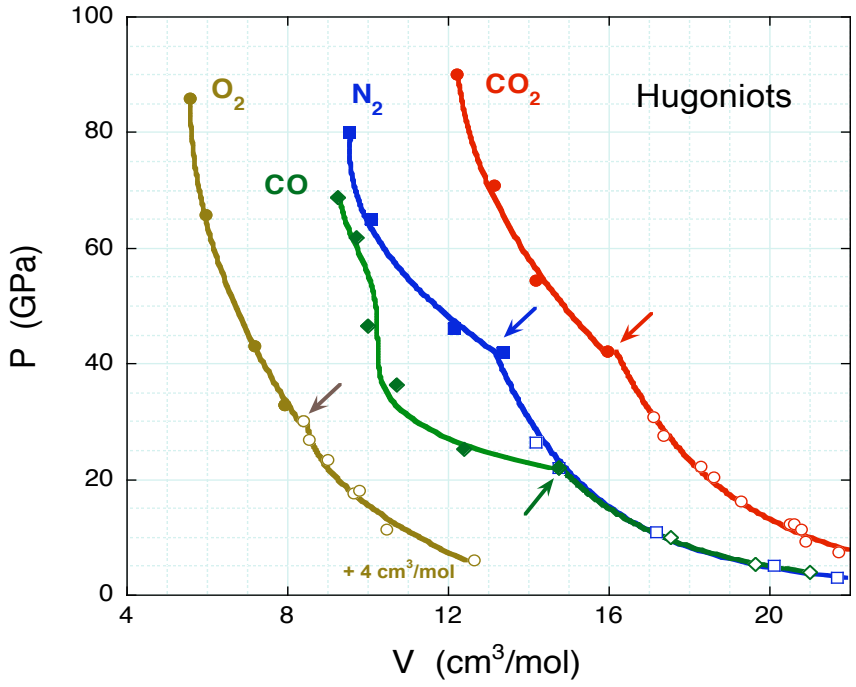


***Figure 1.*** *Hugoniots of selected simple molecular solids, reproduced from the reference 4. Each of these materials exhibits a cusp (indicated by arrow), a strong indication of chemical and/or physical change. Open and closed symbols, respectively, represent unreacted and reacted part of the Hugoniots.*

There are numerous examples, also indicating the increase of chemical instability of unsaturated molecular bonds at high static pressures. The examples include many recent discoveries: covalently bonded nonmolecular phases of nitrogen [8,9], carbon dioxide [10], cyanogen [11], and carbon monoxide [12], charge transferred ionic solids of nitrous dioxide [13,14], oxygen [15], and hydrogen [16], metallic phases of oxygen [17,18, 19], iodine [20, 21], and xenon [22,23], hydrogen bonded extended solids of symmetric ice [24, 25] and hydrogen cyanide [26], and dissociative products of methane [27,28] and aromatic compounds[29]. These fundamental changes in chemical bonding of simple molecular solids may or may not occur reversibly upon the reversal of pressure and temperature, offering the opportunity to understand the materials metastability. These transformations and the associated changes in thermodynamic, mechanical, electronic and magnetic properties are also fundamental to understand the state of matters in the deep interiors of Earth and other planets and the chemistry behind high energetic detonation and combustion.

Modern advances in theoretical and computational methodologies now make possible to explain or even predict novel structures and properties in a relatively wide range of length scales on the basis of thermodynamic stability. These theoretical calculations have been successful, not only to explain the details of materials discovered in experiments such as crystal structures, stabilities, properties, and transition dynamics [30-32], but also to predict new often highly unusual phases that might exist at the extreme conditions. To list a few recent predictions includes super ionic phases of $H_2O$ and $NH_3$ [33], superconducting metallic $H_2$ [34], and nonmolecular $H_2$ fluid [35]. The development or realization of these predicted, potentially useful materials is, however, controlled by the stability of solids as well as the metastablility. In fact, many nanoparticles and surface structures are engineered based on knowledge of their metastability. This makes the experimental confirmation of material in a given stability (or metastability) field the priority in materials research. Furthermore, theoretical calculations using the first principles of physics and chemistry are computationally intensive (because of the intrinsic $N^3$ dependence) and rapidly become challenges as the system gets large and/or the transition takes long, even with the most powerful computational tool available today. In this regard, a close dialog of theory and experiments is the most powerful way to address fundamental issues in high-pressure materials research.

### 1.1. Fundamental Principles of High Pressure Chemistry

The recent discoveries of nonmolecular phases of simple molecular solids [8-29] demonstrate the proof-of-the-principles for producing exotic phases by application of high pressure. More importantly, such a transition from a molecular solid to a denser covalently

bonded framework structure indicates the fundamental principle of high-pressure chemistry. This occurs because electron kinetic energy has a higher density dependence ($\rho^{2/3}$) than that of electrostatic potential energy ($\rho^{1/3}$). As a result, electrons localized within intramolecular bonds become increasingly less stable as density (or pressure) increases and the intermolecular potential becomes highly repulsive (Fig. 2). At high enough pressures, it will essentially lead to physical and chemical changes of molecular solids and modification of their chemical bonds to more delocalized states such as polymeric and metallic solids. This perhaps is the reason for which many unsaturated molecular bonds become unstable above 10 GPa and network structures are ubiquitous at high pressures as found in the crystal structures of diamond, *c*-BN, $\beta$-$C_3N_4$ [36], symmetric-$H_2O$ [24, 25], and $CO_2$ [37].

Three mechanisms may occur at high pressures to delocalize electrons and soften repulsive potentials: (i) the pressure-induced ionization creating attractive electrostatic coulomb interaction, (ii) polymerization delocalizing intramolecular electrons between neighboring molecules, and (iii) metallization completely delocalizing electrons through conduction bands. These processes represent the collective properties of solids, strongly dependent on the intermolecular separation. Therefore, it is likely that these processes occur with increasing pressure as molecular phases → ionic species → polymeric phases → metallic phases, in a way to produce the configuration with more itinerant electrons.

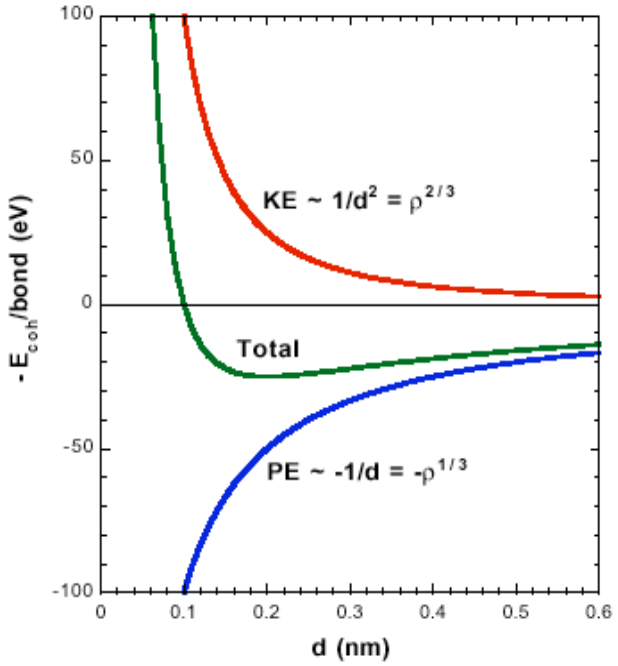


***Figure 2.*** *A conceptual representation of intermolecular energy change as a function of intermolecular distances. The nature of intermolecular potential becomes highly repulsive at a short distance or high density.*

Because of large modification in chemical bonding associated with the molecular-to-nonmolecular phase transition, one might expect large activation energies in the reverse process and thus the nonmolecular product to be metastable even at the ambient condition. Furthermore, these types of extended molecular solids, particularly made of low-Z first and second row elements, are entirely a new class of novel materials that may exhibit interesting properties such as super-hardness [37], optical nonlinearity [10], superconductivity [34, 38-39], high energy density [40], and to name a few. The previous theoretical calculations [40], for example, have predicted that polymeric nitrogen may contain a dramatically enhanced energy density (Energy/Volume) equal to about three times that of HMX (one of the most powerful conventional high explosives available today). Metallic $H_2$ has been predicted to be a high Tc superconductor [34], as are many other low-Z molecular solids like B, Li and S [38, 39] found to be.

## 1.2. Generalized Phase Diagram of Simple Molecule

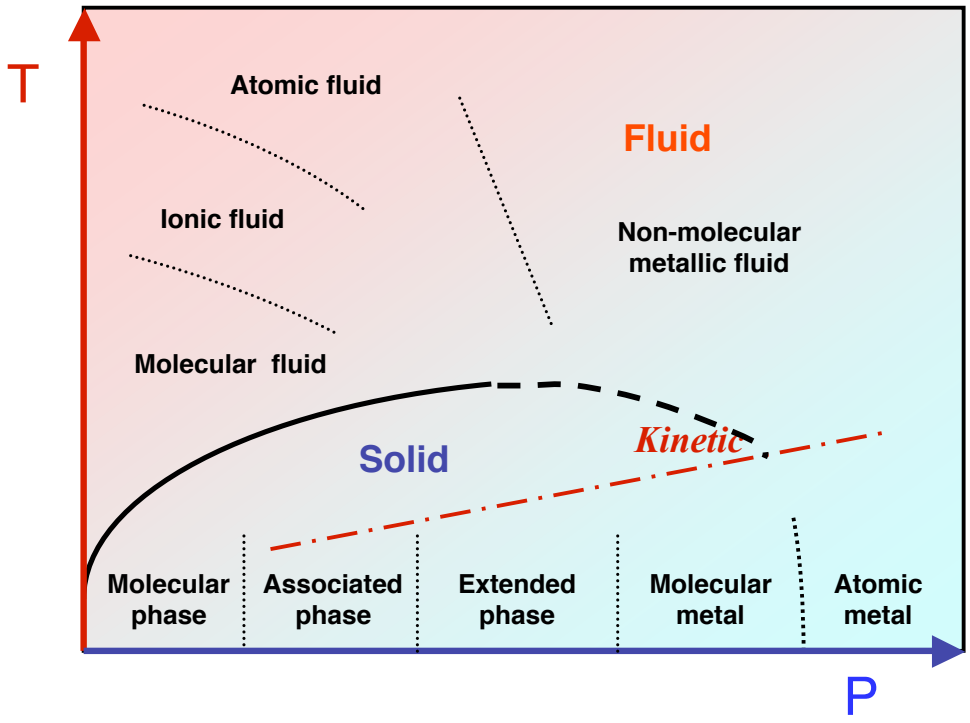


***Figure 3.*** *A conceptual generalized physical/chemical phase diagram of solids at high pressures and temperatures, illustrating the melting maximum and phase boundaries in both solid and fluids*

Figure 3 illustrates several chemical and physical changes of molecular solids occurring at high pressures and high temperatures. At high pressures of 100 GPa, electrons develop

huge kinetic energy (Fig. 2) and, thereby, the core and valance electrons can strongly mix with valence electrons of its own or nearby molecules. Such a core swelling and/or a valence mixing creates an excellent environment for simple molecules to chemically transform into nonmolecular phases such as polymeric and metallic solids. At high pressures of 100 GPa, the mechanical energy ($P\Delta V$) of the molecular system often exceeds an eV, comparable to those of most chemical bonds and certainly enough to induce chemistry acquiring bond scissions. The products are controlled by collective behaviors of molecules, leading to strongly associated phases probably in a pressure range of 10-50 GPa, multi-dimensional polymeric products at around 50 and 100 GPa, and eventually band-gap closing molecular and atomic metals typically above 100 GPa. At sufficiently high pressures of ~1 TPa, most solids will lose their periodic integrities [41] and the system with simple or no core electrons (*e.g*. $H_2$ and He) may even convert into a bare nuclei.

The materials at high temperatures, on the other hand, often transform into an open structure like bcc because of a large increase of entropy [41]. The melting transition is another example of electron delocalization in an simple electron-gas model [42]. In fact, at extremely high pressures where the matter is composed of a bare nuclei, one can expect the melting to occur at zero K [43]. This would result in a melting maximum and a close loop of melting curve as illustrated in Fig. 3. Further increasing temperatures well above the melt will eventually ionize, dissociate or even decompose molecules into elemental atoms [3,4,44,45]. Such a temperature-induced ionization would eventually produce a conducting state of matter if the pressure be sufficiently high [46.47]. This means that the molecular-to-nonmolecular and/or insulator-to-metallic transitions would also form a close loop in the pressure-temperature phase diagram. These close loops of melting and molecular-to-nonmolecular phase lines should intersect at a triple point of intermediate high pressures and temperatures [35, 48]. Therefore, the combined effect of high pressure and high temperature will provide a way of probing a delicate balance between mechanical ($P\Delta V$) and thermal ($T\Delta S$) energies or between pressure-induced electron delocalization and temperature-induced electron ionization, reflected on stabilities of phases and the phase boundaries. These pressure-temperature induced changes are unique, establishing an entirely different set of periodic behaviors in crystal structure and electronic and magnetic properties unfound in the conventional periodic table. In return, this is what makes the "*Mbar chemistry*" unique from any ambient-pressure combinatorial chemistry based on variation of chemical composition and temperature. New opportunities to discover interesting phenomena and exotic materials exist in both liquids and solids at high pressures.

## 2. EXPERIMENTAL TOOLS FOR HIGH PRESSURE RESEARCH

Studies of high-density molecular solids and fluids at the extreme pressure-temperature conditions where molecular solids transform into nonmolecular polymeric and metallic phases are very challenging, because of the difficulties associated with achieving such formidable high pressure-temperature conditions, the absence of *in-situ* structural probe for a minute sample inevitable in static high pressures, and the transient nature of species encountered in dynamic high pressure conditions. With recent developments of high pressure-temperature membrane diamond-anvil cells coupled with micro-probing diagnostic methods available at third-generation synchrotron x-ray sources [49] and modern laser systems [50], these challenges on one hand are rapidly becoming more attainable for static experiments. There are also rapid growing efforts of utilizing a large volume press in high-pressure materials research, made of WC anvils, sintered-diamond anvils, Møssanite anvils [51], Sapphire anvils, or CVD grown large volume anvils [52]. Gas gun, laser, and magnetic drivers, on the other hand, can also be used in high-pressure materials research to investigate the dynamic aspect of material behaviors at high pressures and temperatures. While these dynamic experiments are typically performed to exploit the materials on the Hugoniot states, the method can be modified to provide variable loading that can range from near isentropic all the way to the Hugoniot [53-55] and to utilize modern diagnostic developments capable of probing transient events such as a ps-time resolved x-ray diffraction and a sub-ps laser probes [56].

Shock and static high pressures are complimentary in many aspects including thermal conditions, kinetics, states of stress, rates of loading, etc., all of which could have different implications for materials applications. Because of these differences, the materials behave very differently under shock and static conditions. For example, the materials at shock compressions favor a martensitic transformation than a reconstructive one [57]. Shock-compressed liquid is often found at the *P, T*- conditions well above its melt curve, due to the kinetics associated with forming long-range ordered solids [58]. Large crystals can be grown in static conditions; whereas, shock wave typically results in nanocrystals or amorphous materials. Shock-induced reactions are often dissociative; whereas, the static reactions are typically associative [59]. The shear-band interaction is a typical mechanism for the reactions in shock-compressed solids; whereas, such an interaction is absent in static conditions [60]. Clearly, complementary information from shock- and static- high pressures experiments is critical to gain insight of materials transformation at high pressures and temperatures.

# 3. EXAMPLES OF TRIATOMIC MOLECULAR SOLIDS

There are numerous theoretical and experimental results demonstrating that simple molecular solids transform into nonmolecular phases at high pressures and temperatures, ranging from monatomic molecular solids such as sulfur [61], phosphorous [62] and carbon [63] to diatomic molecular solids such as nitrogen [8, 9, 40], carbon monoxide [12] and iodine [20,21], to triatomic molecules such as ice [24,25], carbon dioxide [10,31,37] and carbon disulfide [64, 65] to polyatomics such as methane [27,28] and cyanogen [11], and aromatic compounds [29]. In this section, we will limit our discussion within a few molecular triatomics: first to review the transformations in two isoelectronic linear triatomics, carbon dioxide and nitrous dioxide, and then to discuss about their periodic analogies to carbon disulfide and silicone dioxide.

## 3.1. Carbon Dioxide: $CO_2$

Carbon dioxide is a good example of material with a richness of high-pressure polymorphs and a great diversity in intermolecular interactions, chemical bonding and crystal structures. The phase diagram of carbon dioxide (Fig. 4) summarizes the physical and chemical changes and their crystal structures (Fig. 5) at high pressures and temperatures. Early high-pressures studies [60, 66-68, 70] established the existence of two molecular solid phases: a cubic (*Pa3*) phase I and an orthorhombic (*Cmca*) phase III, both stabilized by quadruple interactions between the linear molecules [71]. Recent diamond-anvil cell studies [37, 72-74] have discovered three additional phases whose chemical bondings and crystal structures are very different from those of molecular solids. New phases discovered include tetrahedral bonded polymeric phase V ($P2_12_12_1$) like $SiO_2$-tridymite, bent phase IV ($P4_12_12$ or *Pbcn*) like $SiO_2$-cristobalite or a post-stishovite $\alpha$-$PbO_2$, and strongly associated pseudo-six-folded phase II ($P4_2/mnm$ or *Pnnm*) like $SiO_2$-stishovite (or its orthorhombic distortion to a $CaCl_2$-like structure). The evidence of the sixth phase VI [74] has also been reported but its crystal structure and stability field is not well understood. It is also known that carbon dioxide molecules undergo strong chemical changes under shock compression evident from a cusp in shock Hugoniot near 40 GPa and 4500 K (see Fig. 1). Though no chemical change was observed in pure carbon dioxide at high temperatures (at least up to 3000 K) below 30 GPa, an interesting ionic form of carbon dioxide dimer, $CO^{2+}CO_3^{2-}$, was produced by laser heating carbon particles in oxygen to above 2000K at around 10 GPa [75].

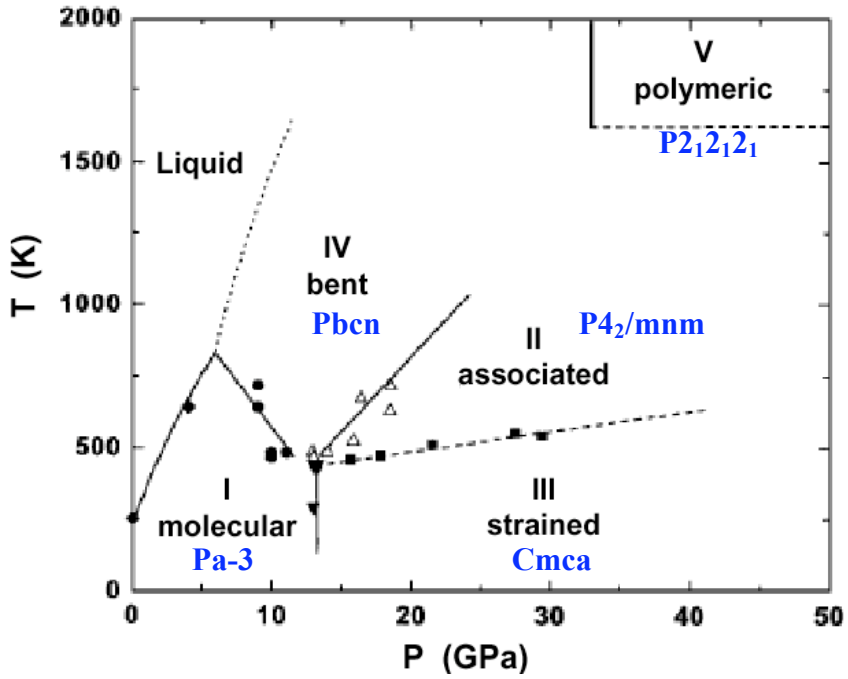


***Figure 4 (top).*** *Phase diagram of carbon dioxide with five polymorphs with 50 GPa and 2000 K. All high temperature phases, II, IV and V, can be stabilized at the ambient temperature over an entire stability range of phase III. This may suggest that phase III is metastability, frozen in only through compression of phase I, and result in four phase boundaries of I through IV being accidentally degenerated at a single thermodynamic point. This phase diagram indicates that pure molecular solid like I is stable only within a limited range of pressure and temperature (less than 10-20 GPa and 500 K) and transforms into non-molecular extended phase V through intermediate phases like II, IV and to some extent highly strained phase III at high pressures.*

***Figure 5 (below).*** *Crystal structure of carbon dioxide polymorphs: (a) a cubic (Pa-3) phase I with four molecules per unit cell. In this structure, carbon atoms at the face centered positions and the molecular axis aligned to the great diagonal direction. (b) a orthorhombic (Cmca) phase III with four molecules per unit cell, a layer structure with all carbons at the face centered positions and all molecules are on the ab-plane. (c) a tetragonal ($P4_2/mnm$) structure with pseudo-six folded carbon atoms with two elongated intramolecular bonded oxygens and four collapsed intermolecular bonded oxygen atoms in the four nearest neighbor molecules. Because of a short oxygen-oxygen contact distance, this phase exhibits an orthorhombic distortion (Pnnm) and dynamic disorder. (d) an orthorhombic (Pbcn) structure with four molecules per unit cell with bent molecular configurations. This phase also shows an elongated intramolecular bonds and a collapsed intermolecular bonds. (5) an orthorhombic ($P2_12_12_1$) structure with eight molecules per unit cell. In this structure, all carbon atoms are four fold coordinated with carbon-oxygen single bonds.*

(a) $CO_2$-I (*Pa-3*)

(b) $CO_2$-III (*Cmca)*

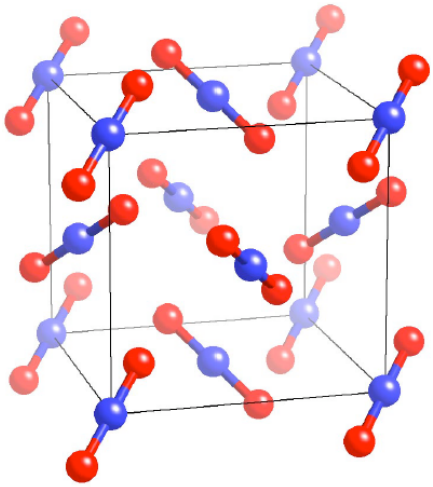

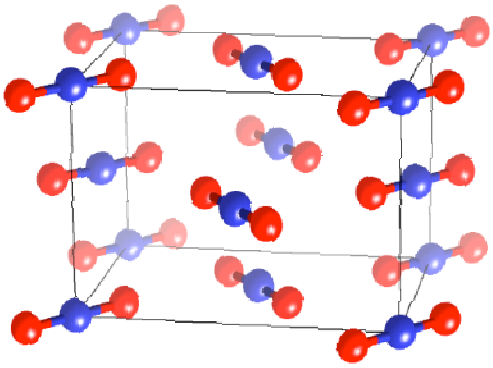

(c) $CO_2$-II ($P4_2/mnm$)

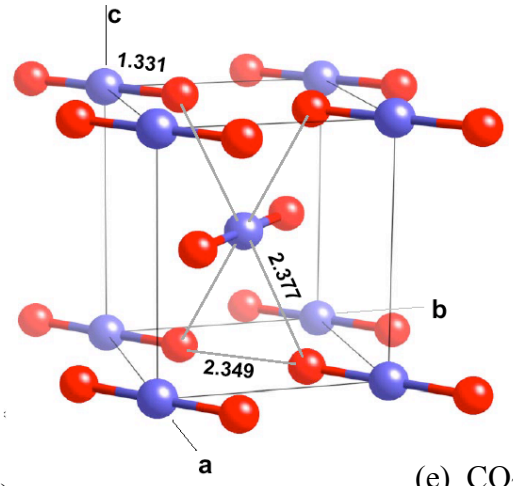


(d) $CO_2$-IV (*Pbcn*)

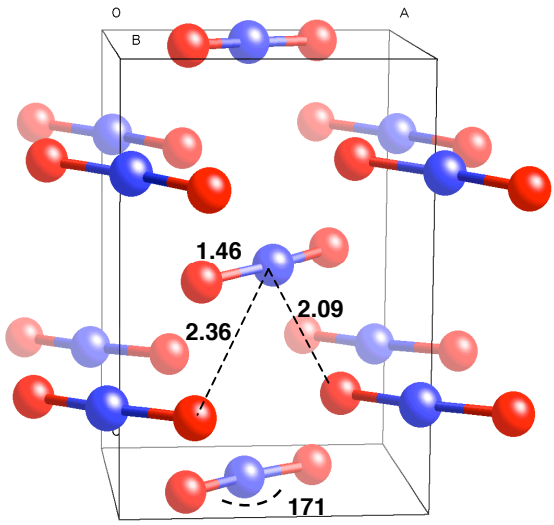


(e) $CO_2$-V ($P2_12_12_1$)

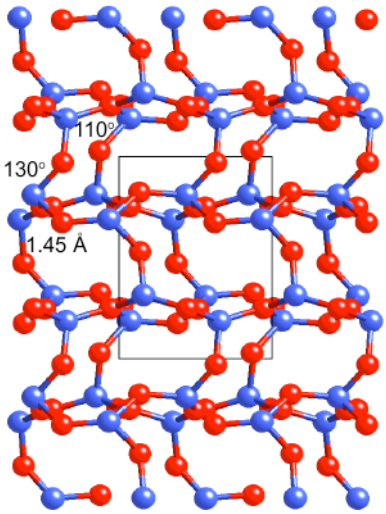

### 3.1.1. Molecular Phase I and III

Carbon dioxide molecule is a simplest form of linear molecular triatomics abundant in nature. At ambient temperatures, it crystallizes into cubic (*Pa-3*) phase I, known as "dry ice", at around 1.5 GPa and then to orthorhombic phase III (*Cmca*) above 12 GPa (see Figs. 4 and 5). Both of these structures commonly appear in many other molecular solids [76,77], for which stabilities have been well understood in terms of the intermolecular quadrupole-quadrupole interaction. In these phases at relatively low pressures below 15 GPa, the nearest intermolecular separation is in a range of 3.0 to 2.5 Å, typically 2 - 2.5 times of the intramolecular C=O bond distance ranging 1.35 – 1.30 Å (all depending on pressure). These values are typical for molecular solids [1].

The crystal structures of these two molecular phases are similar. All carbon atoms are at the face centered positions. Carbon dioxide molecules in phase I are aligned along the great diagonal direction, whereas, those in phase III are aligned approximately along the face diagonal within the ab-plane. As a result, the I III phase transition is associated with only a minor change in molecular rearrangement; that is, a slight tilt of $CO_2$ molecules from the great diagonal to the face diagonal without any apparent discrete change in their specific volumes [9]. This martensitic nature makes the I III phase transition sluggish at ambient temperature, and both phases coexist over an extended pressure range between 12 and 22 GPa. The extended metastability of cubic $CO_2$-I to 22 GPa also reflects its small energy difference from that of $CO_2$-III in this pressure range, and a presence of small lattice strain would prolong the stability of $CO_2$-I well above its stability field as was observed.

There is, however, a subtle but important difference between the two phases. Note that the molecular axis of carbon dioxide is slightly tilted from the exact diagonal direction at 51.7 degree. As a result, oxygen atom in phase III faces approximately the center of C=O bonds, not the carbon atoms of nearest neighbor molecules. Therefore, one may consider the *Cmca* phase as a "paired" layer structure. Such a pairing of molecules in the *Cmca* structure has an important consequence at high pressures (above 20 GPa), converting this phase III to a non-typical molecular solid. It develops high strains in the lattice evident from its characteristic texture and the ability to support a large pressure gradient (~100 GPa/mm at 30 GPa). It also has unusually high bulk modulus of 80 GPa [78] (comparable to that of Si - 87 GPa [79]). Therefore, it is a possibility that molecular phase III is not stable in this pressure range, but the kinetic barrier may preclude any further transformation at the ambient temperature. In fact, this conjecture is supported by its transformation at high temperatures to nonmolecular phase V above 40 GPa and to intermediate phases II and IV above 20 GPa. Further convincing is the fact that all of these

high-temperature phases II, IV and V can be quenched in an entire stability field of $CO_2$-III.

### 3.1.2. Nonmolecular extended phase V

Laser heating the phase III transforms into an extended nonmolecular solid, phase V, above 40 GPa and 1800 K [10]. The vibration spectrum of this phase shows a strong C-O-C stretch mode at around 800 $cm^{-1}$ at 40 GPa, clearly indicating that it is an extended covalent solid made of carbon-oxygen single bonds. Though it occurs above 1800 K, the transition appears to have no strong dependence on temperature. Thus, it is likely that the experimentally observed phase boundary be a kinetic barrier. In fact, the first principles calculation at 0K suggests that such a molecular-to-nonmolecular phase transition would take place above 40 GPa. The phase V can be quenched at the ambient temperature as long as the pressure retains above 10 GPa. Below 10 GPa, it depolymerizes into the phase I, although the remnant of polymeric phase V can be seen at substantially lower pressures down to 1 GPa where $CO_2$ liquidifies or sublimes.

Determining the crystal structure of phase V has been challenging for several reasons, including (i) its coexistence with other phases due to an incomplete transformation of phase III and/or the metastability of other high temperature phase IV and II, (ii) the presence of large lattice distortion and (iii) highly preferred orientation. Nevertheless, the x-ray data indicate that the crystal structure is similar to that of trydimite ($P2_12_12_1$) [37]. In this structure of $CO_2$-V, each carbon atom is tetrahedrally bound to four oxygen atoms. These $CO_4$ tetrahedral units share their corner oxygens to form six-fold distorted holohedral rings with alternating tetrahedral apices pointing up and down the ab-plane. The apices of tetrahedra are then connected through oxygen atoms along the c-axis. This interconnected layer structure of tetrahedra results in the C-O-C angle 130 $(\pm 10)^o$, which is substantially smaller than those of $SiO_2$-tridymites, $174^o$-$180^o$ [80].

It is well known that in $SiO_2$ there is very little energy difference for various polymorphs of tridymite. In addition, there often exists a substantial distortion in the oxygen sublattice of $SiO_2$-tridymite. In fact, recent theoretical calculations have shown that there are a little difference among those candidate structures of $CO_2$-V, including □, □-quartz, *m*-chacopalite, trydimite, coesite, etc.. However, contrary to a wide range of Si-O-Si bond angles in $SiO_2$ from near $180^o$ in tridymite to $145^o$ in quartz [81], all C-O-C bond angles in $CO_2$-V were estimated to be about 130 degrees. Such rigidity in the C-O-C bond angle results in a relatively large distortion in the six-fold holohedra along the ab-plane of $CO_2$-V. It in turn reflects the fact that oxygen atoms in $CO_2$-V are more tightly

bound than in $SiO_2$ and results in a higher covalence and bulk modulus for $CO_2$-V than for any $SiO_2$ polymorphs.

The synthesis of "polymorphic carbon dioxide" resembling $SiO_2$ glass has long been a challenge in chemistry for many reasons such as high strength, high thermal conductivity, wide band gap, high chemical stability, etc.. The high-pressure synthesis of polymeric phase V clearly demonstrates the very existence of $CO_2$ polymer and, more importantly, reveals several interesting properties. It is an optically nonlinear solid, converting infrared light into green light with a high conversion efficient unparallel to any of conventional nonlinear crystals [10]. It also has an extremely low compressibility nearly same with *c*-BN (Table I) and thus is likely super hard [37]. The recovery of this phase V at the ambient condition, however, remains to be a challenge to date.

***Table I***. *The stiffness of carbon dioxide phases in comparison with other covalently materials, showing extremely low compressibilities of nonmolecular carbon dioxide phases.*

| Soilds | ρ (g/cm³) | $B_o$ (GPa) |
|---|---|---|
| Diamond | 3.50 | 450 |
| cubic-BN | 3.48 | 369 |
| $CO_2$-V | 2.90 | 362 |
| $Al_2O_3$ | 4.00 | 239 |
| hcp-Fe | 8.29 | 165 |
| $CO_2$-II | 2.45 | 130 |
| Silicon | 2.33 | 98 |
| $CO_2$-III | 2.22 | 87 |
| $CO_2$-I | 1.75 | 6 |
| δ-$N_2$ | 1.03 | 3 |

### 3.1.3 Intermediate phases II and IV

At 19 GPa, $CO_2$-III transforms to a new phase, $CO_2$-II, above 500 K and then to $CO_2$-IV above 650 K [82]. These transformations are apparent from distinct changes in both visual appearance and Raman spectrum as represented in Fig. 6. The Raman spectrum of quenched $CO_2$-IV exhibits a triplet bending mode $\delta_2$(O=C=O) near 650 $cm^{-1}$, suggesting a broken inversion symmetry because of molecular bending in this phase.

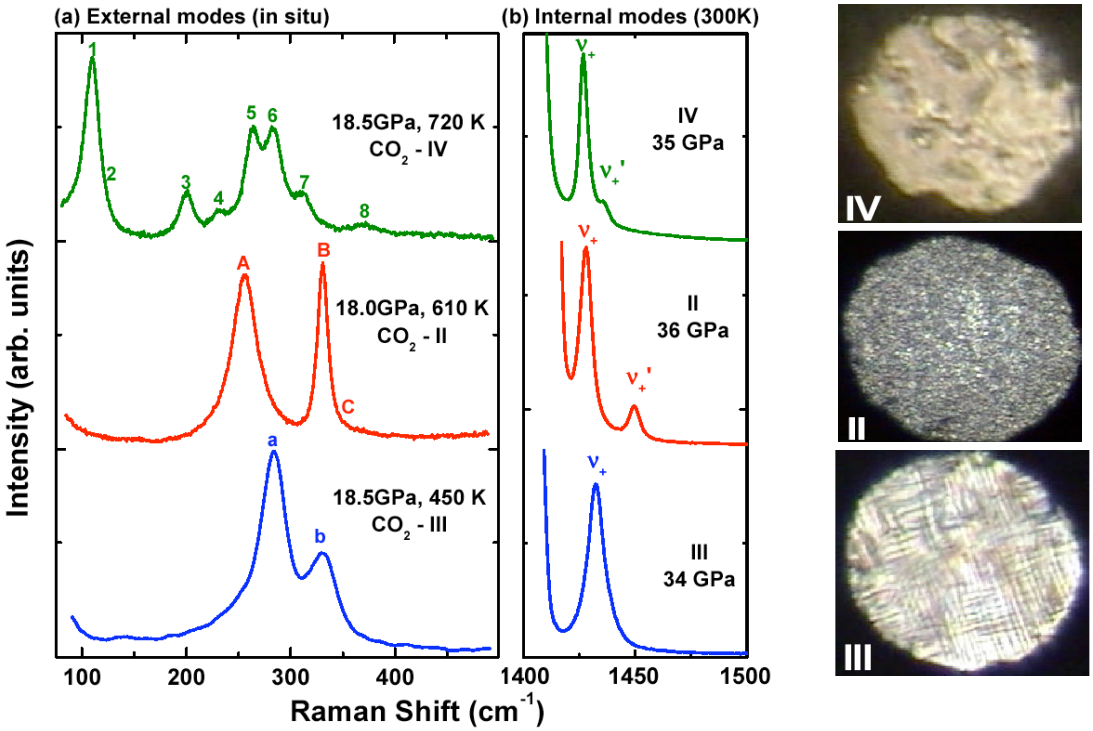


***Figure 6.*** *Characteristic visual appearances and Raman spectra of carbon dioxide phases at high pressures and temperatures, The microphotograph were taken at 18.5 GPa as temperature increases to 450, 610 and 720 K for each phases. Note a large separation of the $\nu_1$ mode of phase II indicates a strong association of $CO_2$ molecules.*

$CO_2$-II crystallizes into a stishovite-like structure (*$P4_2/mnm$*), where carbon atoms are pseudo-six fold coordinated with oxygen atoms: two bonded oxygen atoms at the elongated C=O distance ~1.33 Å and four nonbonded oxygen atoms of nearest molecules at about 2.34 Å. Note that the intermolecular distance is even less than twice the intramolecular distance. Based on the elongated intramolecular bond distance and the collapsed intermolecular distance, the phase II should be considered as an intermediate phase between molecular and nonmolecular solids [73]. Strong molecular association of carbon dioxide molecules in this highly distorted octahedral structure in turn results in a high bulk modulus near $B_o$ = 130 GPa (Table II) and a large separation of symmetric $\nu_1$ vibration (see two bands at around 1450 $cm^{-1}$ of phase II at 36 GPa in Fig. 6). Furthermore, this is a layer structure with an extremely short oxygen-oxygen contact distance, 2.35 Å, in the ab-plane, resulting in a tetragonal-to-orthorhombic (*Pnnm*, *$CaCl_2$*-like) distortion and the dynamic disorder evident in both Raman and x-ray data.

The crystal structure of $CO_2$-IV can be interpreted in terms of two plausible models: the *$P4_12_12$* ($\alpha$-$SiO_2$ cristobalite) and the *Pbcn* ($\alpha$-$PbO_2$, post-stishovite). Carbon dioxide

molecules are bent slightly more in the *Pbcn* phase (<C-O-C = 160 degree) than in the $P4_12_12$ (171 degree). In fact, the Raman spectrum of phase IV [83] clearly includes the $\square_2$ bending modes, typically forbidden in a linear molecule. Thus, it too suggests the bending of $CO_2$ molecules. Because of dipole interactions, the intermolecular interactions are expected to be even stronger in this phase than that of phase II. For both models, the intramolecular C-O bond is increased to 1.5 (±0.1) Å at the distance of C-O single bond, whereas the intermolecular C..O distance is reduced to around 2.1 (±0.2) Å. The bending and elongation of the molecular units suggest that phase IV is also an intermediate state between the molecular and non-molecular extended phases. Therefore, it is apparent that the molecular-to-nonmolecular transformation in carbon dioxide occurs gradually via intermediate phases IV and II.

Both phases II and IV can be quenched at ambient temperatures over the entire stability field of phase III. This result indicates that the phase III is likely a metastable phase. Interesting changes have also observed from the quenched phase IV in particular. The 650 $cm^{-1}$ bending modes rapidly soften with increasing pressure, indicating an enhanced intermolecular interaction among neighboring bent $CO_2$ molecules. At 80 GPa, the low-frequency vibron collapses into high-frequency phonons, and $CO_2$-IV becomes an extended amorphous solid, another form of nonmolecular $CO_2$. Upon laser heating the quenched phase IV, $CO_2$-IV transforms into polymeric $CO_2$-V above 30 GPa. Note that the IV□ V transition pressure 30 GPa is substantially lower than that of the III□ V transition 40 GPa. It is probably due to the bent configuration of $CO_2$-IV, which lowers the activation barrier of the polymerization.

### 3.1.4. Ionic solids

At relatively low pressures below 10 GPa where carbon dioxide remains purely molecular. Carbon-oxygen double bonds are highly stable and no transformation has been observed to 3000 K in phase I. On the other hand, there has been an experimental evidence for which the direct elementary reaction of carbon and oxygen at about 2000 K and 9 GPa yields an nearly transparent ionic product of carbon dioxide dimer [75]. The fact that the ionic carbon dioxide dimer does not form directly from molecular carbon dioxide, implying an existence of a large activation barrier for the dimerization pathway. However, once formed at high P and T, the dimer can be quenched to ambient temperature at high pressures.

The Raman spectrum of quenched products (Fig. 7) consists of the symmetric stretching of excess □-$O_2$ at 1585 $cm^{-1}$, two Fermi-resonance bands of $CO_2$ at 1270 and 1400 $cm^{-1}$, and three new additional sharp bands at 734, 1079, and 2242 $cm^{-1}$. The systematic of the latter three bands are very similar to those of nitrosonium nitrate $NO^+NO_3^-$, an ionic dimer

of nitrogen dioxide. This similarity suggests that the products also include a species with carbonates and carbosonium, $CO^{2+}CO_3^{2-}$. The vibrations of carbonate ions appears at 713 and 1082 $cm^{-1}$ in $CaCO_3$ [84], and the CO vibration appears about 2150 $cm^{-1}$ at 5 GPa [85]. Electronic structure calculations for $CO^{2+}$ [86, 87] suggest that there are several low lying states of $CO^{2+}$, whose vibrational frequencies vary between 1000 and 2000 $cm^{-1}$. The yield of ionic dimer in this sample is small; other samples show nearly complete conversion (*vida infra*, the 9 GPa trace in Fig. 6).

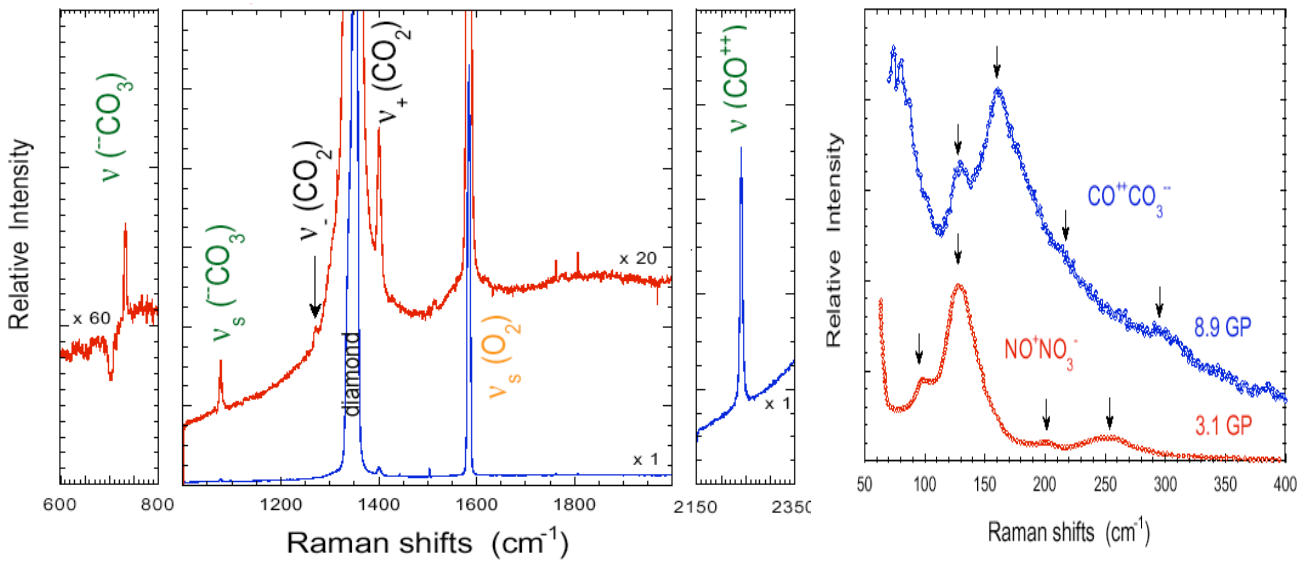


***Figure 7.*** *Raman spectra of $CO^{2+}CO_3^{2-}$ quenched from the elementary reactions of C and $O_2$ at 9 GPa and 2000 K, in (a) internal and (b) external vibrational regions.*

Figure 7 also compares the lattice phonons of the C-$O_2$ products with those of $NO^+NO_3^-$ and shows striking similarities in the number of bands, band shapes, widths and intensities. Differences in the peak positions can be attributed to different pressures, force constants, and reduced masses. Similarities of vibrons and lattice phonons between $NO^+NO_3^-$ and the C-$O_2$ reaction products imply that they have similar molecular configurations, $CO^{2+}CO_3^{2-}$, and similar crystal structures. The crystal structure of $CO^{2+}CO_3^{2-}$ has not been determined as yet; that of $NO^+NO_3^-$ has been determined to be aragonite-like structure (will be discussed in the sections).

### 3.1.5. Dissociative solids

Shock-compressed carbon dioxide exhibits a strong slope change in the Hugoniot (recall Fig. 1), a clear indication of chemical reaction, at around 40 GPa and estimated

temperature of 4500 K [1]. The previous theoretical calculation has confirmed that it is indeed due to chemical dissociation of carbon dioxide to elementary products such as diamond and oxygen. In recent diamond-anvil cell experiments [74], the similar dissociative products, lonstaleite diamond and oxygen, have also been observed from the quenched products after laser-heating of $CO_2$ samples at 67 GPa. The transition temperatures were estimated to be about 2500 K at 35 GPa, substantially lower than the estimated shock transition temperature 4500 K.

### 3.2 Nitrous Oxide: an Electronic Analog

$CO_2$ and $N_2O$ are isoelectronic, linear triatomics with similar molecular weights, melting temperatures and quadrupole moments. Although $N_2O$ has no inversion symmetry, it has been shown to resonate between two bonding configurations with opposing dipole moments: $^{-}N{=}N^{+}{=}O$ and $N{=}N^{+}{=}O^{-}$ [88]. As a result, the net dipole moment of nitrous oxide is negligible compared to its substantial quadrupole moment [89, 90] at relatively low pressures. Therefore, one can find a close parallelism between the phase diagrams of $N_2O$ in Fig. 8 [91] and $CO_2$ discussed above (Fig. 4). However, note that such a close phase parallelism is maintained mainly in a molecular regime. Upon breaking or weakening of N=O (C=O) bonds at high pressures and temperatures, the different nature of carbon and nitrogen enhances the ionic character in $N_2O$ phases and eventually leads to ionization of $N_2O$, instead of the polymerization as seen in $CO_2$.

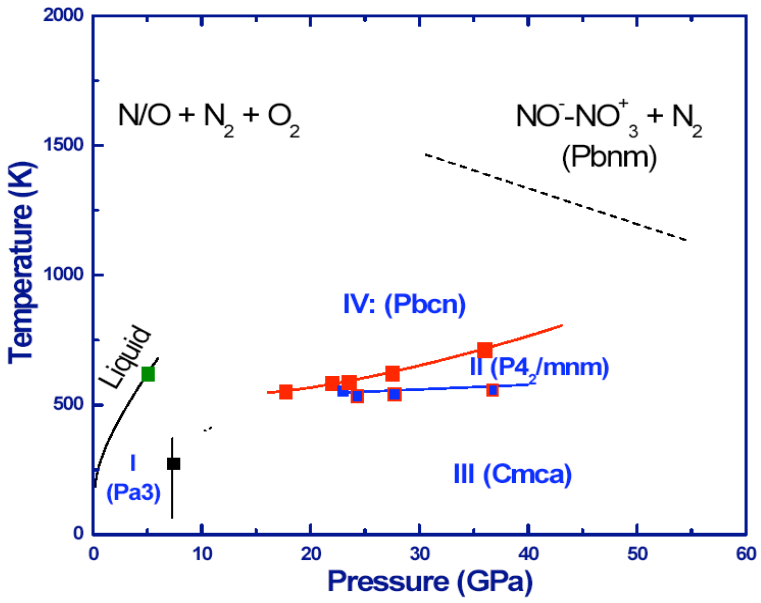


***Figure 8.*** *Phase diagram of nitrous oxide*

### 3.2.1 The phase diagram of $N_2O$

In the absence of dipole ordering, $N_2O$ molecules are oriented randomly and crystallize in the same configurations as $CO_2$ [92] as phase I (*Pa3*) at 1 GPa and phase III (*Cmca*) above ~5 GPa. At high temperatures, there exist two additional $N_2O$ phases (labeled II and IV in Fig. 8). Above ~600 K, phase II stabilizes above 23 GPa in a relatively narrow temperature range 10-30 K. Phase IV, on the other hand, is obtained by heating either phase III below 23 GPa, or phase II at higher pressures. These transformations can be readily observed by abrupt changes in the visual appearance of the sample and in the Raman spectrum, similarly to the case of $CO_2$ phases.

While the one-to-one phase analogy between $CO_2$ and $N_2O$ is maintained at relatively low pressures and temperatures, these materials develop significant differences with increasing pressure and temperature. For example, at ambient temperatures, $N_2O$-III remains stable to at least 135 GPa, whereas $CO_2$-III becomes highly unusual above 20 GPa and becomes unstable above 40 GPa with respect to its polymeric phase V. The crystal structure of high-temperature phase IV also exhibits a subtle but important difference between $N_2O$ and $CO_2$. That is, the center nitrogen atoms in $N_2O$-IV occupy the face-centered-cubic (*fcc*) sites; whereas the carbon atoms in $CO_2$-IV deviate from the *fcc* packing and form zigzag chains. This difference results in a perfect layer structure and a relatively large bending angle $132^o$ in $N_2O$, but in a large buckling of $CO_2$ layers and a substantially smaller bending angle $170^o$ in $CO_2$. This divergence is due to the difference in ionicity (or covalency) between $N_2O$ and $CO_2$. Such a difference in ionicity, in turn, leads to further significant divergence in their chemistry at high pressures and temperatures. That is, $N_2O$ disproportionates into ionic $NO^+NO_3^-$ and $N_2$ [13, 14] whereas $CO_2$ polymerizes into an extended covalent solid above 35 GPa and 2000 K [10, 72].

### 3.2.2 Ionization and dissociation

Laser-heating of $N_2O$-III at lower pressures, 10-20 GPa, to about 2000 K (Fig. 9) produces a more complicated set of products, consisting of $\delta$-$N_2$ (the doublet near 2365 $cm^{-1}$), $\delta$-$O_2$ (doublet at 1650 $cm^{-1}$), $NO^+NO_3^-$ (730, 835, 1095, and 2250 $cm^{-1}$), nitrogen-oxygen products (features between 750 $cm^{-1}$ and 1070 $cm^{-1}$). Subsequent heating of the ionic product also results in a similarly complex set of dissociation products. Therefore, it is apparent that the ionic phase $NO^+NO_3^-$ further dissociates into $N_2$ and $O_2$. In fact, the ionization is always accompanied by dissociation when $N_2O$-III is laser-heated at pressures below 30 GPa, whereas no evidence for further dissociation of $NO^+NO_3^-$ was observed to 3370 K at higher pressures. These results suggest that the dissociation

temperature of the ionic dimer increases with increasing pressure. Note also in Fig. 9c the splitting of the oxygen stretching mode, indicating that the oxygen is dissolved in $\delta$-$N_2$ (Pm3n) [93]. This splitting is due to a vibration-vibration resonance transfer between molecules at two types of molecular sites of $\delta$-$N_2$ [94]. The relative intensities of the components of the doublet vary with pressure and composition[21], on which basis we estimate the oxygen content of the $\delta$-$N_2$ in Fig. 9c to be about 10 %.

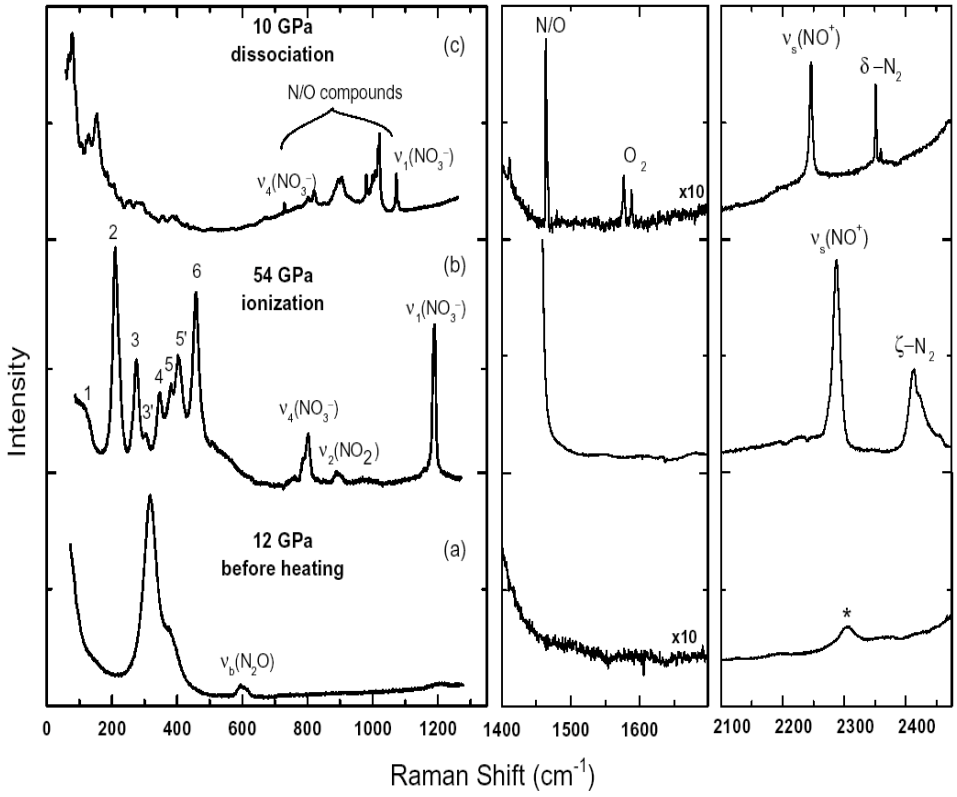


***Figure 9.*** *Raman spectra of $N_2O$-IIIL (a) before and (b, c) after laser-heating, showing the pressure-induced reactions to (b) the ionization products of $NO^+NO_3^-$ and $\delta$-$N_2$ at 54 GPa and (c) the dissociation products $\delta$-$N_2$ containing dissolved $O_2$, N/O-compounds, and $NO^+NO_3^-$ at 10 GPa*

Both the ionic and dissociative reaction products (Fig. 9b and 9c, respectively) are quenchable at room temperature at all pressures studied (between 10 and 55 GPa). The ionic phase ($NO^+NO_3^-$) is stable in a wide pressure region to 55 GPa, the maximum pressure applied. No reverse transition of $NO^+NO_3^-$ to the molecular phases of $N_2O_4$, $N_2O$, or $NO_2$ was observed even below the $N_2O$-I/III transition pressure 4-5 GPa. This is contrarily to the high pressure-temperature phases of $CO_2$ (phases II, III, IV, and V and its ionic dimer phase [95]), all of which transform back to the phase I (*Pa3*) near 11 GPa. Note that the splitting of the $\delta_4$ mode above 35 GPa, probably resulted from the anisotropic strain developed in the lattice.

### 3.2.3. Novel ionic crystal

A rigorous determination of the crystal structure of $NO^+NO_3^-$ has not been made to date, because of several experimental challenges such as the coexistence of by-products like δ-$N_2$ (*Pm3n*) and $N_2O$-III (Cmca) and their highly preferred orientation. Nevertheless, based on the Le Bail fit, the x-ray diffraction data of $NO^+NO_3^-$ can be explained in terms of an orthorhombic cell with a plausible space group of either *Pnma* or $Pn2_1a$. Note that the Pnma structure is analogous to the aragonite, $CaCO_3$, as occurred in other nitrates such as $KNO_3$ or $NH_3NO_3$ [96].

$NO^+NO_3^-$ is an extremely high density ionic solid with the density ~2.7 g/cc at the ambient condition. Figure 10 compares room-temperature isotherms for $N_2O$-III and $NO^+NO_3^-$ to 55 GPa with those of $CO_2$-III and $CO_2$-V. At pressures below 15 GPa, $N_2O$-III is relatively soft initially ($B_o$= 10.9 GPa), as is typical of molecular solids, e.g., $N_2O$-I ($B_o$=7.9) and $CO_2$-I ($B_o$=6.2). At higher pressures, $N_2O$-III rapidly stiffens and its compression curve becomes essentially identical to that of $CO_2$-III. The ionic phase of $NO^+NO_3^-$, however, behaves quite differently from the non-molecular phase $CO_2$-V. $NO^+NO_3^-$ is substantially softer ($B_o$=45.0 GPa) than polymeric $CO_2$-V ($B_o$=362 GPa) [37]. As a result, $NO^+NO_3^-$ becomes denser than $CO_2$-V above 12 GPa despite its lower density at the ambient pressure. The higher density of $NO^+NO_3^-$ than $CO_2$-V at high pressures probably reflects a more efficient packing of the ion pairs in $NO^+NO_3^-$. It is probably due to relatively strong attractive columbic interaction of the ion pairs, in contrast to very stiff covalent bonds of $CO_2$-V with its low-coordination structure. This result is also consistent with the higher number of nearest neighbors in $NO^+NO_3^-$ than $CO_2$-V; for example, each nitrosonium ($NO^+$) ion has six nearest nitrate ions, whereas each carbon atoms in $CO_2$-V has only four nearest oxygen atoms.

The inset of Fig. 10 compares the molar volumes of $N_2O$-III with the ionic and dissociative products. Above 5 GPa, the mixture of $NO^+NO_3^-$ and $N_2$ [97] has smallest molar volume and thus is favored over both $N_2O$-III and the dissociative mixture of $N_2$ and $O_2$ [98]. On the other hand, the molar volume of the $N_2$ and $O_2$ mixture becomes smaller than that of δ-$N_2O$ above 56 GPa and, based on the extrapolation, of the mixture of $NO^+NO_3^-$ above 130 GPa. This result thus suggests that the ionization is primarily driven by densification at high pressures, whereas the dissociation observed between 10 and 30 GPa results from the combined effects of densification and entropy increase at high pressures and temperatures. This conclusion is also consistent with the presumption that the dissociation would require higher temperature than the ionization.

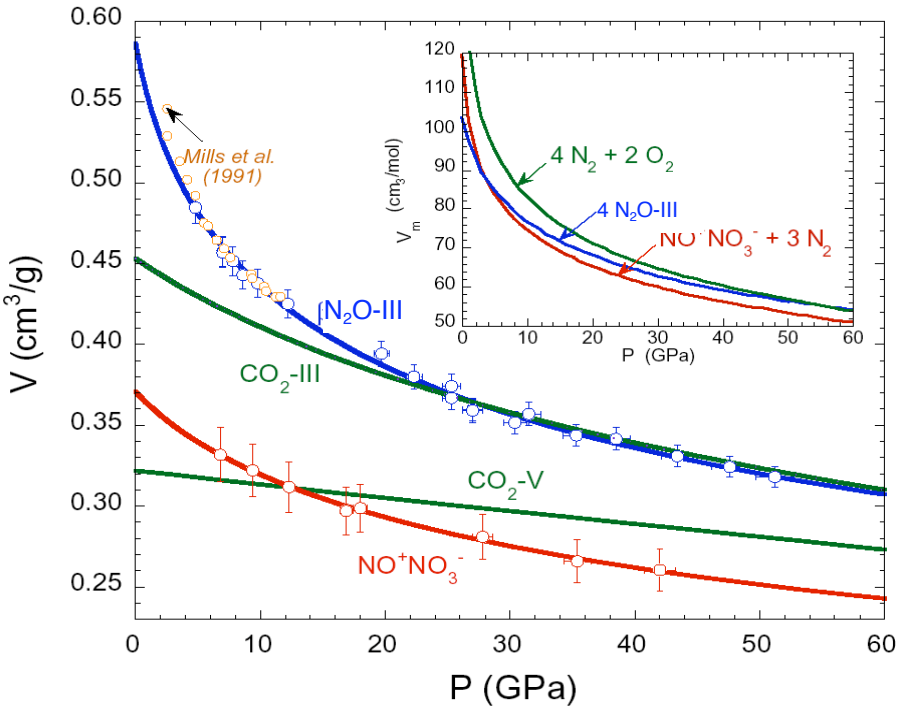


***Figure 10.*** *Pressure-volume plots of $NO^+NO_3^-$ in comparison with $N_2O$ and $CO_2$ phases. (Inset) Molar volumes of $N_2O$ in comparison with ionic and dissociated products.*

### 3.3 Carbon Disulfide: a Periodic Analog

Carbon disulfide is also another example of $CO_2$ analog, a centro-symmetric linear triatomic molecule with a similar valence electronic structure. The phase diagram of carbon disulfide is shown in Fig. 11. At room temperature, $CS_2$ molecules crystallizes into an orthorhombic (*Cmca*) structure at ~0.5 GPa [99]. While this structure is identical to those of $CO_2$-III and $N_2O$-III, it is interesting to note that the cubic *Pa-3* structure seen in $CO_2$-I and $N_2O$-I is absent in the phase diagram of $CS_2$. Nevertheless, it is still consistent with the periodic structural variation with pressure; for example, the absence of the graphite structure in silicon and the second-row $CO_2$ transforming to the structures of the third-row compound $SiO_2$ at high pressures. Furthermore, as in the cases of $CO_2$-III, the $CS_2$ molecules in the *Cmca* phase behave cooperatively and lead to strong chemical reactions at high pressures and high temperatures. In fact, there are many other examples showing strong collective behaviors in the *Cmca*, including $X_2$ [100], $H_2$-III [101], $Li_2$ [102], etc.

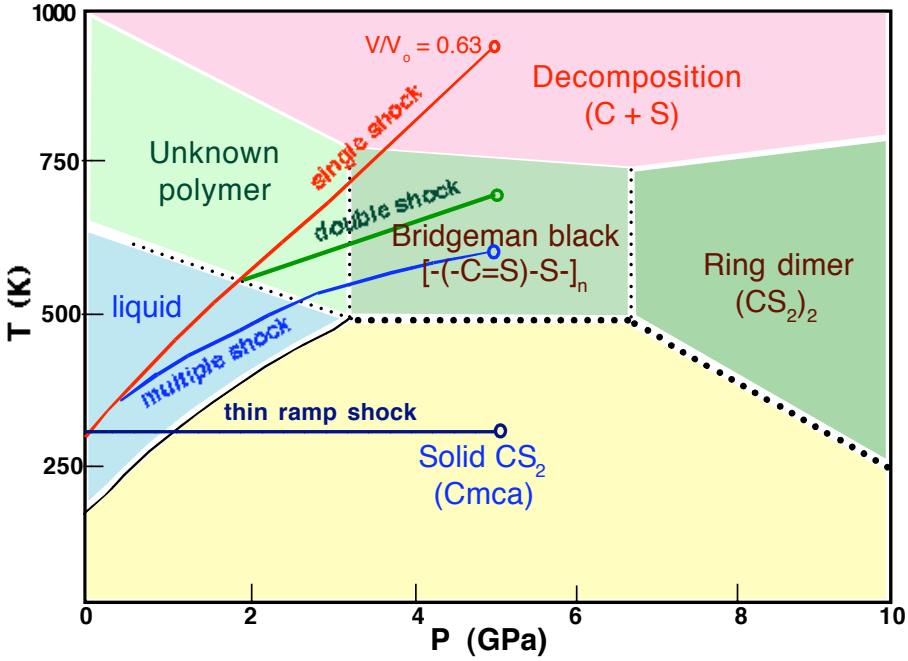


***Figure 11.*** *Phase diagram of carbon disulfide, showing several reaction zones at high pressures and temperatures. The pressure-temperature conditions of various shock wave experiments are also reproduced to highlight the similarity observed in reaction products between shock and static high pressure experiments.*

Bridgman was the first to report the chemical transformation of carbon disulfide to a black polymer under static high pressure-temperature condition (~5.5 GPa and 450 K) [103]. However, Agnew and coworkers [104] later found that the chemistry of $CS_2$ is actually substantially more complicated at high pressures and temperatures as illustrated in Fig. 11. Several reaction zones were identified, all of which contain the mixtures of multimer products of carbon dioxide. Note that at the ambient temperature carbon disulfide transforms into a dimeric product above 9 GPa, signifying the dimeric pairing of the *Cmca* structure.

The chemical reaction of $CS_2$ have also been studied under various (single [105], double [106], and multiple [107]) shock conditions, which follow different thermal paths as illustrated in Fig. 11. For example, $CS_2$ molecules under single shock conditions decompose to carbon and sulfur [105]; whereas, they behave collectively under multiple shock conditions [108, 109]. These studies found that the primary effect of pressure and temperature on $CS_2$ is the □-electron delocalization. Such a □-electron delocalization induces the molecular bending, evident from the appearance of "T-band" in absorption [110], which could be a precursor to the chemical reaction. Based on the cooperative

behavior of $CS_2$ and the absorption spectral changes, the reaction was suggested to be an associative one to $CS_2$ multimer and/or Bridgman black polymer, similar to those observed under the static conditions. The collective behavior and polymerization of $CS_2$ molecules are in a way analogous to those of $CO_2$.

### 3.4 Silicon Dioxide: a Periodic Analog

Despite a huge difference in the electronic structure, the crystal structures of $CO_2$ phases exhibit a great degree of similarity with those of many $SiO_2$ polymorphs as shown in Fig. 12. The examples include stishovite-like $CO_2$-II (*$P4_2/mnm$*) [73], β-cristobalite-like $CO_2$-IV (*$P4_12_12$ or Pbcn*) [72], tridymite-like $CO_2$-V (*$P2_12_12_1$*) [37], and even α-cristobalite-like $CO_2$-I (*Pa-3*). While the structures of $CO_2$ phases are (or close to) isostructural to those of $SiO_2$ polymorphs, the nature of chemical bonding is clearly different between $CO_2$ and $SiO_2$ polymorphs. With increasing pressure and temperature, the intermolecular bonding in $CO_2$ phases, for example, increases from nearly non-bonding in the phase I to approximately a half-bonding in phases II and IV and to a full covalent bonding in phase V.

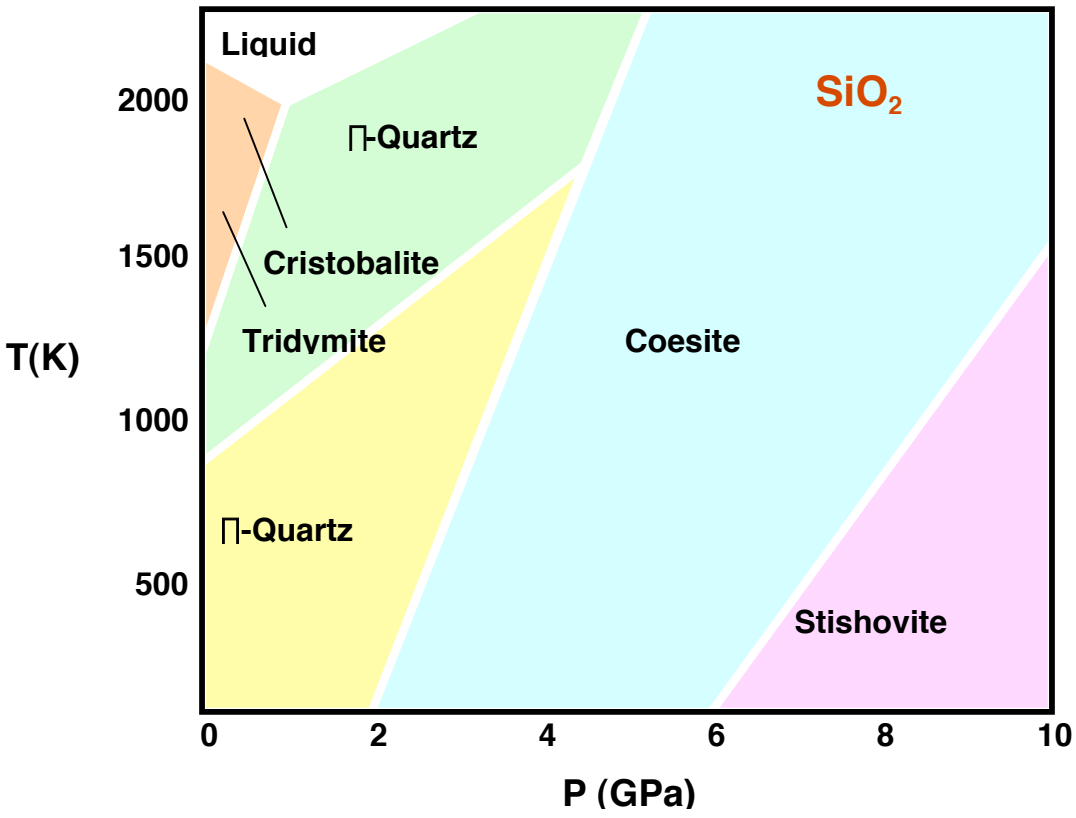


***Figure 12.*** *Phase diagram of $SiO_2$*

The crystal structure and transformation of $CO_2$-II also exhibits subtle difference from stishovite: (1) because of high covalency in C-O bonds [111-113], the O-C-O and O-C-O angles are more rigid and favor 110-130 degrees, which contrasts with a wider range of angles, 90 to 180 degrees, observed in various $SiO_2$ polymorphs [114, 115]. (2) There are no nearby *d*-bands in carbon, which makes it difficult to stabilize nonbonding electrons of oxygen atoms at pressures below 100 GPa. As a result, the transition of $CO_2$-II to a "perfect" six-folded extended phase is limited at these intermediate pressures. Instead, the lattice develops various distortions like the tetragonal-to-orthorhombic distortion and bending of linear molecules, which precede a transition to a four-fold carbon dioxide-V phase. (3) Finally, $CO_2$-II appears at lower pressures than four-fold $CO_2$-V, whereas six-fold stishovite appears at substantially higher pressures than four-fold quartz and coesite. Clearly, it reflects the intermediate nature of $CO_2$-II between molecular and extended solids.

## 4. CONCLUDING REMARKS

While the pressure-induced electron delocalization explains qualitatively the molecular-to-nonmolecular phase transition, the detailed mechanisms are substantially more complex because of the existence of intermediate phases, metastability, kinetics, and lattice strain. For all triatomics molecules discussed above, the molecular phases are only stable within a limited range of pressures (<10 GPa) and temperatures (<500 K) and that, at higher pressures and temperatures, they transform into molecular configurations with more itinerant electrons. For example, molecular $CO_2$ phase I and III first transform to pseudo-six fold coordinated phase II ($P4_2/mnm$ or $Pnnm$) and bent phase IV ($Pbcn$ or $P4_12_12$), both with elongated molecular bonds and compressed intermolecular distances, and finally to a fully extended phase V ($P2_12_12_1$), made of four-fold coordinated carbon atoms. These experimental results suggest that the electron delocalization occurs gradually, *via* intermediate phases (II, IV and III to an extent) to a fully extended covalent solid (V). The formation of intermediary phases lowers the barrier to breaking the strong C=O molecular double bonds to form singly bonded tetrahedral $CO_4$ structures.

Similarly, molecular $N_2O$ phase I and III transform to the intermediary phase II ($P4_2/mnm$) and IV ($Pbcn$) and then disproportionates to an ionic product of $NO^+NO_3^-$ and

$N_2$. The increase of ionicity in $N_2O$ leads to the ionic solid, that again occurs gradually *via* dipole ordered $N_2O$-III and IV phases.

However, theoretical descriptions of such a gradual electron delocalization through intermediate phases have been challenges. Recent total energy calculations of $CO_2$ [116], for example, assert a different picture that the high-pressure, "intermediate" phases may be strictly molecular and have entirely different phase stabilities. This calculation, however, fails to account for the stability of the bent phase IV (*Pbcn*) and, instead, suggests that a molecular *Cmca* structure (experimentally found at the ambient temperature) occupies the entire stability field of phase IV (experimentally found only at high temperatures). This description advocates an extended stability domain for molecular $CO_2$ and seems to imply that the molecular-to-nonmolecular transition occurs rather *abruptly* at the phase boundary between phases III and V.

While the existence and stability of bent configuration in $CO_2$, $N_2O$, and $CS_2$ are apparent [72, 83, 91, 107], theoretical descriptions of such phases also face challenges [116] and result in substantially higher energy, ~ several eV, than their linear configuration. Nevertheless, it is not surprising, considering the fact that the bent configuration is stabilized only by their collective behaviors at high pressures. Without strong molecular association (seen in the phase II and III and, to an extent, the paired layer phase III at high pressures), the bent configuration may simply represent an excited state of these triatomics, which is bent and several eV higher than the linear ground states. Furthermore, considering that transformation kinetics plays an important role in determining the phase stability of both $N_2O$ and $CO_2$ (and very likely other molecular compounds), any calculation aiming to predict their phase stabilities *must* include molecular dynamics simulations of a large number of structural configurations and reaction paths in addition to the minimum energy calculations.

## 6. ACKNOWLEDGEMENT

The experimental works reported in this article have previously been done in collaboration with Drs. V. Iota, J. Park and H. Cynn at the LLNL; Prof. M.F. Nicol at the UNLV; Prof. Y. Gupta at the WSU. This work has been supported by the LDRD and PDRP programs at Lawrence Livermore National Laboratory, University of California under the auspices of the U.S. Department of Energy under Contract No. W-7405-ENG-48.

## 7. REFERENCES


1. L. Pauling, Nature of the Chemical Bond (Cornell University Press, Itaca, N.Y.1940).
2. A. Jayarama, Rev. Mod. Phys. 55, 65 (1983)
3. R.J. Hemley, Ann. Rev. Phys. Chem. 51. 763 (2000).
4. W.J. Nellis, A.C. Mitchell, F. H. Ree, M. Ross, N.C. Holmes, R.J. Trainor, J. Chem. Phys. 95, 5269 (1991); W.J. Nellis, F.H. Ree, M. vsn Thiel, and A.C. Mitchell, J. Chem. Phys. 75, 3055 (1981); W.J. Nellis, N.C. Holmes, A.C. Michell, and M. van Thiel, Phys. Rev. Lett. 53, 1661 (1984); W.J. Nellis and A.C. Mitchell, J. Chem. Phys. 73, 6137 (1980).
5. R.L. Mills, B. Olinger, and D.T. Cromer, J. Chem. Phys. 84, 2837 (1986)
6. D.T. Cromer, R.L. Mills, D. Schiferl, and L.A. Schwalbe, Acta Crystalogr. B 37, 8 (1981).
7. H. Schneider, W. Hafner and A. Wokaun. J. Chem. Phys. 96, 8046 (1992).
8. M.L. Erements, R.J. Hemley, H.K. Mao, E. Gregoryanz, Nature 411, 170 (2001).
9. A.F. Goncharov, E. Gregoryanz, H.K. Mao, Z. Liu, R.J. Hemley, Phys. Rev. Lett. 85, 1262 (2000).
10. V. Iota, C.S. Yoo, H. Cynn, Science 283, 1510 (1998).
11. C.S. Yoo and M. F. Nicol, J. Phys. Chem.90, 6726 (1986); *ibid* 90, 6732 (1986).
12. A. Katz, D. Schiferl, R.L. Mills, J. Phys. Chem. 88, 3176 (1984).
13. M. Somayazulu, A. Madduri, A.F. Goncharov, O. Tschauner, P.F. McMillan, Phys. Rev. Lett. 87, 135504 (2001).
14. C.S. Yoo, V. Iota, H. Cynn, M. Nicol, J.H. Park, T. Le Bihan, and M. Mezouar. J. Phys. Chem. B 107, 5922 (2003).
15. M. Nicol and K. Syasson, Phys. Rev. B28, 1201 (1983)
16. R.J. Hemley, Z.G. Soos, M. Hanfland, and H.K. Mao, Nature 369, 384 (1994).
17. A.F. Goncharov, E. Gregoryanz, R.J. Hemley, and H. K. Mao, Phys. Rev. B68, 100102 (2003).
18. F.A. Gorelli, L. Ulivi, M. Santoro, and R. Bini, Phys. Rev. Lett. 83, 4093 (1999).
19. S. Desgreniers, Y.K. Vohra, A.L. Ruoff, J. Phys. Chem. 94, 1117 (1990).
20. K. Takemura, S. Minomura, O. Shinomura, Phys. Rev. Lett. 49, 1772 (1982).
21. K. Takemura, K. Sato, H. Fujihisa, O. Mitsuko, Nature 423, 971 (2003).
22. R. Reichlin, M.Ross, S. Marin and K.A. Goettel, Phys. Rev. Lett. 56, 2858 (1986).
23. K.A. Goettel, J.H. Eggert, and I.F. Silvera, Phys. Rev. Lett. 62, 665 (1989).
24. K. Aoki, H. Yamawaki, M. Sakashita, H. Fujihita, Phys. Rev. B54, 15673 (1996).
25. Ph. Pruzan, I.C. Chervin, B. Canny, J. Chem. Phys. 99, 9842 (1993).
26. K. Aoki, S. Usuba, M. Yoshida, Y. Kakudate, K. Tanaka, and S. Fujiwara, J. Chem. Phys. 89, 529 (1988).
27. M. Ross, Nature 292, 435 (1981).
28. L.R. Benedetti, J.H. Nguyen, W.A. Caldwell, H. Liu, M. Kruger, R. Jeanloz, Science 286, 100 (1999).
29. L. Ciabini, M. Santoro, R. Bini, V. Schettino, J. Chem. Phys. 116, 2928 (2002).
30. F. Ancilotto, G.L. Chiarotti, S. Scandolo, E. Tosatti, Science 275, 1288 (1997).
31. S. Serre, C. Cacvaxxoni, G.L. Chiarotti, S. Scandolo, E. Tosatti, Science 284, 788 (1999)
32. J. Dong, J.K. Tomfohr, O.F. Sankey, Phys. Rev. B62, 14685 (2000).
33. C. Cavazzoni, G.L. Chiarotti, S. Scandolo, E. Tosatti, M. Bernasconi, M. Parrinello, Science 283, 44 (1999).
34. C.F. Richardson and N.W. Ashcroft, Phys. Rev. Lett. 78, 118 (1997).

35. S. Scandolo, Proc. Natl. Acad. Sci. U.S.A. **100**, 3051 (2003).
36. A.Y. Liu and M.L. Cohen, Science 245, 842 (1989).
37. C. S. Yoo, H. Cynn, F. Gygi, G. Galli, V. Iota, M. Nicol, S. Carlson, D. Hauserman, and C. Mailhiot, Phys. Rev. Lett. 83, 5527 (1999).
38. M. Eremets, V.V. Struzhkin, H.-K. Mao, R.J. Hemley, Science 293, 272 (2001).
39. V.V. Struzhkin, M. Eremetsm W. Gan, H.-K. Mao, R.J. Hemley, Science 298, 1213 (2002)
40. C. Mailhiot, L.H. Yang, and A.K. McMahan, Phys. Rev. B46, 14419 (1992).
41. D. A. Young, Phase Diagrams of the Elements. (UC Press, CA, 1991).
42. D.M. Ceperley and B.J. Alder, Phys. Rev. Lett. 45, 566 (1980).
43. D.A. Kirzhnits, Usp. Fiz. Nauk 104, 489 (1971); Sov. Phys. Usp. 14, 512 (1972)
44. L.B. Da Silva et al., Phys. Rev. Lett. 78, 483 (1997)
45. M.D. Knudson, D.L. Hanson, J.E. Bailey, C.A. Hall, and J. R. Asay, Phys. Rev. Lett. 87, 225501 (2001)
46. R. Chau, A.C. Mitchell, R.W. Minich, and W.J. Nellis, Phys. Rev. Lett. 90, 245501 (2003).
47. S.T. Weir, A.C. Mitchell, W.J. Nellis, Phys. Rev. Lett. 76, 1860 (1996).
48. Bonev, submitted (2004)
49. G. Shen, M.L. Rivers, Y. Wang, and S. R. Sutton, Rev. Sci. Instrum. 72, 1273 (2001).
50. F. Datchi, R. LeToullec and P. Loubeyre, J. Appl. Phys. 81, 3333 (1997).
51. J.-A. Xu and H.-K. Mao, Science 290, 783 (2000).
52. W.L. Mao, et al., Appl. Phys. Lett. 83, 5190 (2003).
53. C.S. Yoo and Y.M. Gupta, J. Chem. Phys. 93, 2082 (1990)
54. C.A. Hall et al., Rev. Sci. Instrum. 72, 1 (2001).
55. G.E. Duvall and R.A. Graham, Rev. Mod. Phys. 49, 523 (1974).
56. A.M. Lindenberg, et al., Phys. Rev. Lett. 84. 111 (1999).
57. D.J. Erskine and W.J. Nellis, Nature 349, 317 (1991)
58. C.S. Yoo, J.J. Furrer, G.E. Duvall, S.F. Agnew, and B.I. Swanson, J. Phys. Chem. 91, 6577 (1987).
59. J.J. Dick, R.N. Mulford, W.J. Spencer, D.R. Pettit, E. Garcia, D.C. Shaw, J. Appl. Phys. 70, 3572 (1991); J.J. Dick, J. Phys. Chem. 97, 6195 (1993).
60. C.S. Yoo and W.J. Nellis, Science 254, 1489 (1991); C.S. Yoo, W.J. Nellis, M.L. Sattler, aand R.G. Musket, Appl. Phys. Lett. 61, 273 (1992).
61. V.V. Struzhkin, R.J. Hemley, H.-K. Mao, Y. A. Timofeev, 390, 382 (1997).
62. Y. Katayama, T. Mizutani, W. Utsumi, O. Shimonura, M. Yamakata, K. Funakoshi, Nature 403, 170 (2000).
63. F.P. Bundy and J.S. Kasper, J. Chem. Phys. 46, 3437 (1967); F.P. Bundy, Physica 156A, 169 (1989).
64. P. W. Bridgman, Proc. Am. Acad. Arts Sci. 74, 399 (1942)
65. S.F. Agnew, R.E. Mischke. B.I. Swansen, J. Phys. Chem. 92, 4201 (1988); S.F. Agnew, B.I. Swansen, D.G. Eckhart, in Shock Wave in Condensed Matter, edited by Y. M. Gupta (Plenum, New York, 1986), p 221.
66. P.W. Bridgman, Proc. Am. Arts. Sci. 72, 207 (1938).
67. R.C. Hanson and L.H. Jones, J. Chem. Phys. 75, 1102 (1981).
68. B. Olinger, J. Chem. Phys. 77, 6255 (1982).
69. R.C. Hanson, J. Phys. Chem. 89, 4499 (1985).
70. K. Aoki et al., Science 263, 356 (1994).
71. B. Kuchta and R. Etters, Phys. Rev. B47, 14691 (1993).

72. J.-H. Park, C.S. Yoo, V. Iota, H. Cynn, M.F. Nicol, and T. Le Bihan, Phys. Rev. B 68, 014107 (2003).
73. C. S. Yoo, H. Kohlmann, H. Cynn, M. F. Nicol, V. Iota, and T. Le Bihan, Phys. Rev. B 65, 104103 (2002).
74. O. Tschauner, H.-K. Mao, and R.J. Hemley, Phys. Rev. Lett. 87, 75701 (2001)
75. C.S. Yoo, Science and Technology of High Pressure, edited by M. H. Manghnani, M.F. Nicol, (University Oress, Hyberadad, India, 2000), vol. 1, p 86.
76. C.A. English, J.A. Venables, Proc. R. Soc., London A 340, 57 (1974).
77. J.A. Venables and C.A. English, Acta Crystallogr. B30, 929 (1974).
78. C.S. Yoo, et al., Phys. Rev. Lett. 83, 5527 (1999).
79. E. Knittle, Handbook of Physical Constants, edited by T. Ahrens (AGU, Washington D.C., 1995), p98-142.
80. H. Graetsch and O.W. Florke, Z. Kristallogr. 195, 31 (1991).
81. R.F. de Dombal and M.A. Carpenter, Eur. J. Mineral 5, 171 (1998).
82. V. Iota and C.S. Yoo, Phys. Rev. Lett. 86, 5922 (2001).
83. C.S. Yoo, V. Iota, and H. Cynn, Phys. Rev. Lett. 86, 447 (2001).
84. A. Anderson, The Raman Effect, vol. 2, p 911 (Mercel Dekker, Inc., New York, 1973).
85. A. Katz, D. Schiferl, M.J. Mill, J. Phys. Chem. 88, 3176 (1984).
86. P. Lablanquie, J. Delwiche, D.J. Gubb0Frabskin, I. Benner, P. Morin, K. Ito, J.H.D. Eland, J.M. Robbe, G. Gandara, J. Fournier, P.G. Fournier, Phys. Rev. A 40, 5673 (1989).
87. N. Correia, A. Flores-Riveros, K. Helenelund, L. Asplund, U. Gelius, J. Chem. Phys. 83, 2035 (1985).
88. L. Pauling, Nature of the Chemical Bond (Cornell University, Ithaca, 1940).
89. B. Kuchta and R.D. Etters, J. Chem. Phys. 95, 5399 (1991).
90. D.E. Stogryn and A. P. Stogryn, Mol. Phys. 11, 371 (1966).
91. V. Iota, J.-H. Park and C.S. Yoo, Phys. Rev. B69, 064106 (2004)
92. R.L. Mills, B. Olinger, D.T. Cromer, and R.L. LeSar, J. Chem. Phys. 95, 5392 (1991).
93. B. Baer and M.J. Nicol, J. Phys. Chem. 94, 1073 (1990).
94. D.T. Cromer, R.L Mills, D. Schiferl, L. Schwalbe, Acta Crystallogr. B37, 8 (1981).
95. C.S. Yoo, Science and Technology of High Pressure, edited by M. H. Manghnani, M.F. Nicol, (University Oress, Hyberadad, India, 2000), vol. 1, p 86
96. M. Somayazulu, A. Madduri, A.F. Goncharov, O. Tschauner, P.F. McMillan, H.K. Mao, R.J. Hemley, Phys. Rev. Lett. 87, 135504 (2001).
97. R.W.G. Wyckoff, Crystal Structures, 2nd ed., (John Wiley & Sons, New York, 1964), vol. 2, Ch. VII.
98. M. Hanfland, M. Lorenzen, C. Wassilew-Reul, F. Zontone, Rev. High Press. Sci. Technol. 7, 787 (1998); also, see the ESRF Web page by M. Hanfland, 2000.
99. S.F. Agnew, R.E. Mischke, and B.I. Swansen, J. Phys. Chem. 92, 4201 (1988).
100. Y. Fujii, et al., Phys. Rev. Lett. 63, 536 (1989).
101. J. B. Neaton and N.W. Ashcroft, Nature 400, 141 (1999).
102. J.B. Neaton and N.W. Ashcroft, Nature 400, 141 (1999); M. Hanfland, K. Syassen, N.E. Christensen and D.L. Novikov, Nature 408, 174 (2000).
103. P.W. Bridgman, Proc. Am. Acad. Arts Sci. 74, 399 (1942).
104. S.F. Agnew, R.E. Mischke, and B. I. Swanson, J. Phys. Chem. 92, 4201 (1988).
105. R.D. Dick, J. Chem. Phys. 52, 6021 (1970).
106. S.A. Sheffield and G.E. Duvall, J. Chem. Phus. 79, 1981 (1983); *ibid*, 81, 3048 (1984).
107. C.S. Yoo, G.E. Duvall, J.J. Furrer, and R. Granholm, J. Phys. Chem. 93, 3012 (1983).

108. C. S. Yoo and Y. M. Gupta, J. Phys. Chem. 94, 2857 (1990).
109. C. S. Yoo and Y. M. Gupta, J. Chem. Phys. 93, 2082 (1990).
110. Ch. Jungen, D.M. Malm, Can. J. Phys. 51, 1471 (1973).
111. C. S. Yoo, H. Cynn, F. Gygi, G. Galli, V. Iota, M. Nicol, S. Carlson, D. Hauserman, and C. Mailhiot, Phys. Rev. Lett. 83, 5527 (1999).
112. B. Holm, R. Ahuju, A. Belomoslike, and B. Johansson, Phys. Rev. Lett. 85, 1258 (2000).
113. J. Dong, J.K. Tomfohr and O.F. Sankey, K. Leinenweber, M. Somayazulu, and P.F. McMillan, Phys. Rev. B61, 5967 (2000).
114. R.M. Hazen, L. W. Finger, R.J. Hemley, and H.K. Mao, Solid State Commun. 72, 507 (1989).
115. H. Gratsch and O.W. Förke, Z. Kristallogr. 195, 31 (1991).
116. S.A. Bonev, F. Gygi, T. Ogitsu, and G. Galli, Phys. Rev. Lett. 91, 065501 (2003)